J Mater Sci: Mater Med (2015) 26:105
DOI 10.1007/s10856-015-5435-1

Biocompatible elastin-like click gels: design, synthesis and characterization

Ana M. Testera · Alessandra Girotti · Israel González de Torre · Luis Quintanilla · Mercedes Santos · Matilde Alonso · José Carlos Rodríguez-Cabello

Received: 19 June 2014 / Accepted: 23 November 2014 / Published online: 7 February 2015

Abstract Elastin-like recombinamer click gels (ELR-CGs) for biomedical applications, such as drug delivery or tissue engineering, have been developed by taking advantage of the click reaction (CuAAC) in the absence of traditional crosslinking agents. ELRs are functionalized with alkyne and azide groups using conventional chemical techniques to introduce the reactivity required to carry out the 1,3-dipolar cycloaddition under mild biocompatible conditions, with no toxic by-products and in short reaction times. Hydrogels with moduli in the range 1,000–10,000 Pa have been synthesized, characterized, and tested in vitro against several cell types. The cells embedded into ELR-CGs possessed high viability and proliferation rate. The mechanical properties, porosity and swelling of the resulting ELR-CGs can easily be tuned by adjusting the ELR concentration. We also show that it is possible to replicate different patterns on the hydrogel surface, thus allowing the use of this type of hydrogel to improve applications that require cell guidance or even differentiation depending on the surface topography.

A. M. Testera · A. Girotti · I. G. de Torre · L. Quintanilla · M. Santos · M. Alonso · J. C. Rodríguez-Cabello (✉)
Bioforge Group, University of Valladolid, Edificio I+D, Paseo de Belén, 11, 47011 Valladolid, Spain
e-mail: roca@bioforge.uva.es

A. M. Testera · A. Girotti · I. G. de Torre · L. Quintanilla · M. Santos · M. Alonso · J. C. Rodríguez-Cabello
Biomedical Research Networking Center in Bioengineering, Biomaterials and Nanomedicine (CIBER-BBN), Valladolid, Spain

1 Introduction

New biomaterials are currently required to satisfy the needs and expectations of researchers in the bioscience and biotechnology fields. The desirable features of such materials include biocompatibility, specific mechanical properties, cell-friendly behaviour, non-toxic degradation products, and ease of handling. The development of functional materials often involves the generation of well-defined micro- and nanopatterned surfaces. The design and development of systems with a well-defined topographical biochemical activity and controlled mechanical properties is a hot research topic due to their potential biomedical applications [1, 2]. Cell behaviour can be conditioned by a specific and well-defined topography of the material surface, either alone or in combination with specific bioactivity, thus leading to a promising strategy for controlling cellular organization and function in tissue engineering [3, 4]. For instance, topographical patterns have been used to facilitate cell adhesion [5], direct cell migration [6], enhance cell proliferation [7], and control cell differentiation [8], and, according to the work of Engler et al. [9], surface stiffness can also be used to modify the cell phenotype.

Elastin-like recombinamers (ELRs) are protein-based polymers obtained by recombinant DNA technologies, thus allowing the bioproduction of protein polymers with well-defined, complex and controlled sequences. ELRs can include different bioactive sequences [10], such as those for cell adhesion and proliferation or sequences sensitive to enzymes [11]. These materials are based on the repetition of short peptides considered to be building blocks in natural elastin [12]. The wide range of interesting properties exhibited by this family of polymers, for instance their extraordinary biocompatibility, excellent mechanical

properties (similar to those of natural elastin), acute self-assembly and thermosensitive behaviour, should be highlighted [10–13]. The latter is characterized by a critical temperature, known as the transition temperature in aqueous solution (Tt), which is associated with the occurrence of a conformational reorganization in this material. Thus, whereas the polymer chains are soluble in water below Tt, above this temperature they form nano- and micro-aggregates and become insoluble in a completely reversible process.

The Cu(I)-catalysed 1,3-dipolar cycloaddition reaction (CuAAC) between azides and alkynes, which is probably the most prominent example of "click chemistry" [14, 15], was discovered independently in 2002 by the groups of Meldal [16], and Sharpless [17] and is compatible with most functional groups present in proteins and peptides, thereby ruling out the need for protecting groups. This Hüisgen reaction combines high specificity with quantitative yield, a lack of side reactions and toxic by-products, short reaction times, and high tolerance towards other functional groups present in the molecule. As alkynes and azides are remarkably stable within biological systems, click chemistry has been widely employed in drug discovery [18], bioconjugation with proteins [19] and DNA [20], cell surface labelling [21], surface modifications with ELRs [22], amongst other molecules, and for hydrogel synthesis [23, 24]. Some studies have provided evidence of the potential use of ELR-based hydrogels as a scaffold to promote tissue regeneration in vitro due to their low endotoxicity [24], low cytotoxicity and absence of antigenic properties upon implantation [25–27]. In particular, in the field of cartilage tissue engineering, the synthesis and accumulation of a cartilaginous matrix for both encapsulated cartilage cells [28] and human adipose tissue-derived stem cells [29] in vitro has been reported.

In this paper elastin-like recombinamer-click gels (ELR-CGs) are obtained under mild, physiological conditions by exploiting the advantageous properties of the click reaction. Specifically, two modified ELRs including azide or alkyne groups in their structure are processed to obtain chemically covalently cross-linked hydrogels, which are characterized by scanning electron microscopy (SEM), porosity, equilibrium swelling ratio, and rheological properties. The porous structure and favourable thermoresponsiveness of the resulting ELR-CGs are also evaluated. Topographically micropatterned structures with different features are processed by a biocompatible, simple and straightforward method known as the replica moulding [30–32] procedure, which opens up the future possibility of controlling cellular organization and function in tissue engineering as well as the development of cell-based biomedical systems. Finally, the cytocompatibility of these new ELR-CGs will be demonstrated by way of viability assays with several cell lines (HFF-1, MSCs and HUVECs). This cytocompatibility will be demonstrated using both surface and 3D cultures.

2 Materials and methods

All reagents used were of analytical grade. They were purchased from Aldrich Co. and used as received.

2.1 ELR bioproduction

The ELRs used herein were constructed using standard genetic-engineering techniques. Thus, they were produced using cellular systems for genetically engineered protein biosynthesis in Escherichia coli and purified using several cycles of temperature-dependent reversible precipitations [33]. The purity and molecular weight of the ELRs were verified by sodium dodecyl sulfate polyacrylamide gel electrophoresis (SDS-PAGE) and matrix-assisted laser desorption/ionization time-of-flight (MALDI-TOF) mass spectroscopy using a Voyager STR apparatus from Applied Biosystems. Amino acid composition analysis was also performed. Additional characterization of ELRs was accomplished using infrared spectroscopy, differential scanning calorimetry (DSC) and nuclear magnetic resonance (NMR) techniques.

The two ELRs employed were VKVx24, a structural polymer lacking a bioactive sequence and with the amino acid sequence:

MESLLP VG VPGVG [VPGKG(VPGVG)5]23 VPGKG VPGVG VPGVG VPGVG VPGV, and HRGD6, a polymer containing the adhesion sequence (RGD) and with the amino acid sequence [34]:

MGSSHHHHHHSSGLVPRGSHMESLLP [(VPGIG)2(VPGKG)(VPGIG)2]2AVTGRGDSPASS[(VPGIG)2(VPGKG)(VPGIG)2]2.

2.2 Chemical modification of ELRs

The ELRs were chemically modified by transformation of the ε-amine group present in the lateral chain of the lysine residue to bear the groups required for hydrogel formation using click chemistry techniques. The specific modifications are described below.

2.3 Synthesis of azide-bearing ELRs

A substitution reaction was carried out using triflic azide as nucleophile. Triflic azide solution was freshly prepared in situ prior to each reaction as previously described by Lundquist et al. [35] NaN3 (5 eq.) was dissolved in 14 mL of Milli-Q water and 17.5 mL of CH_2Cl_2 added. The

reaction mixture was cooled in an ice-water bath and a solution of triflic anhydride (1 eq.) added dropwise at 4 °C while stirring. The resulting mixture was stirred vigorously at 0 °C for 1 h and then at room temperature for another hour. The crude reaction mixture was decanted and the aqueous phase washed with dichloromethane (2 × 10 mL). The combined organic phases were then washed with saturated Na_2CO_3 solution (10 mL). The resulting azide-containing solution was employed directly without further purification. A solution containing triflic azide was added dropwise to a solution of the ELRs (2 g,VKVx24 or HRGD6, 1 eq.) in 24 mL of milli-Q water with sodium carbonate (1.5 eq) and copper(II) sulfate (0.01 eq) at 0 °C. Methanol (4 mL) was then added and the reaction allowed to run overnight at room temperature. The organic solvents were subsequently eliminated under reduced pressure and the polymer purified by dialysis at 4 °C, followed by lyophilisation to yield a white solid. The transformation was corroborated by MALDI-TOF, IR spectroscopy, amino-acid composition determination, and DSC (Data not shown).

2.4 Synthesis of acetylene-bearing ELRs

Chemical modification of the ELR (VKVx24 or HRGD6) was carried out to obtain an ELR with a pendant alkynyl group. Thus, pentynoic anhydride was synthesized from pentynoic acid (2 eq.) in a 1:1 mixture (v/v) of dichloromethane and diethyl ether in the presence of dicyclohexylcarbodiimide (1 eq.). Ten equivalents of pentinoic anhydride and five equivalents of ethylendiaminecarbodiimide (EDAC) were added to a solution of ELR (1 eq.) in 5 mL of trifluoroethanol (TFE). The reaction mixture was stirred for 3 days at room temperature. After this time the functionalized polymer was precipitated into diethyl ether, washed with additional diethyl ether fractions, and dried under reduced pressure. The modified ELR was solubilized in cold water, purified by exhaustive dialysis against water (3 × 25 L), and lyophilized to yield a white product (89 %). Chemical characterization of the polymer by MALDI-TOF and 1H NMR spectroscopy confirmed total conversion of the free amine group of the biopolymer (data not shown).

2.5 ELR-CHG formation

Different amounts of ELR-alkyne and modified ELR-azide were dissolved in milli-Q water to a final polymer concentration of 25, 50, 100 and 125 mg/mL with an alkyne/azide molar ratio of 1:1. After mixing the above aqueous solutions, sodium ascorbate and aqueous copper(II) sulfate ($CuSO_4$) solution were added as reagents to initiate the crosslinking reaction between the alkyne and azide groups at 4 °C. An azide: copper(II): ascorbate molar ratio of 12:1:3 (optimization process not shown) was used for all reactions. The mixture was vigorously stirred and injected into moulds (diameter: 13.5 mm; height: 2 mm) at 4 °C for 5 min, and then 1 h at r.t., in order to finish the gelification process. Finally, all hydrogels were carefully removed and washed with milli-Q water.

The chemical process for obtaining ELR-CG hydrogels from ELRs is summarised in the scheme shown in Fig. 1. It should be noted that covalent crosslinking is based on the reaction between azide and alkyne groups. Three replicates for each concentration of each hydrogel were prepared for analysis using any of the instrumental methods reported in this work. A preliminary characterization based on IR spectroscopy and DSC was performed (data not shown).

2.6 Micropatterned hydrogels fabricated by replica moulding

The replica moulding method was carried out using micropatterned polydimethylsiloxane (PDMS) substrates as moulds. The PDMS prepolymer and curing agent were thoroughly mixed at a 10/1 (w/w) ratio then degassed for 1 h. The mixture was then cast onto different patterned silicon masters with different topographical features. Specifically, hexagonal pillars [width (w) = 100 μm, spacing (s) = 100 μm], square pillars (w = s = 40 μm and w = s = 100 μm), and grooves (w = 20 μm, s = 100 μm). The step height of the microfeatures was 5 μm for the pillars and grooves. The mixture was cured at 65 °C for 1 h, then the PDMS was carefully peeled off from the silicon wafer and used as a mould. Micropatterned hydrogels were obtained in a one-step process by pouring the mix of aqueous polymer solutions (concentration = 50 mg/mL) with sodium ascorbate and $CuSO_4$ solution, in the proportions previously described, on top of the PDMS mould, at 4 °C. After heating the system from 4 to 25 °C, then leaving it at this temperature for 1 h, the hydrogels were peeled off. Their surface topography was observed, with no prior treatment or manipulation, by optical microscopy, using a Nikon ECLIPSE 80i light microscope, and by scanning electron microscopy (SEM) in low vacuum mode.

2.7 Cell culture

Paraformaldehyde (ref. P6148) and Triton X-100 (ref. T9284) were purchased from Sigma-Aldrich. Normal Human Adipose-Derived Mesenchymal Stem Cells (hMSCs, ref R7788-115) basal medium Dulbecco's modified Eagle's medium (DMEM, ref 31966-021), fetal bovine serum (FBS ref. 16000-044), penicillin streptomycin solution (ref. SV30010), trypsin–EDTA (ref. SV30010), DPBS (ref.

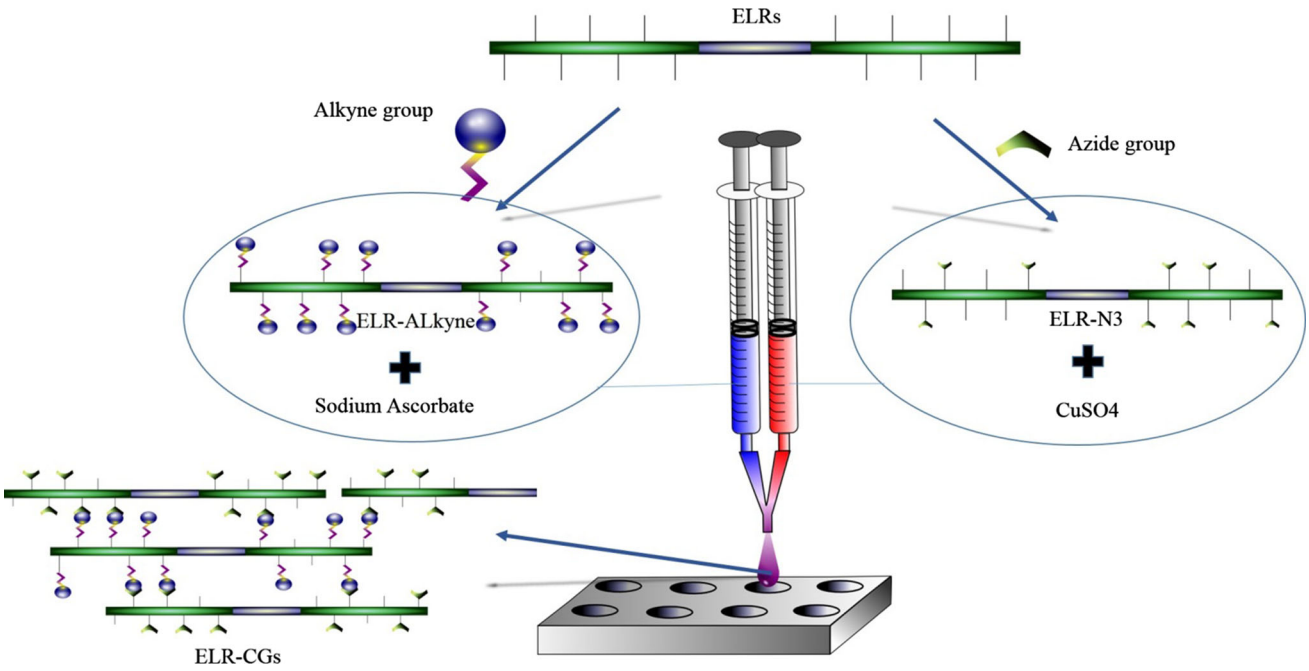

Fig. 1 Scheme showing ELR-CG formation as bi-component system

14190-136), HEPES (ref. 15630049), Trypan Blue stain 0.4 % (ref. 15250061), Alexa Fluor 488 phalloidin (ref. A12379), LIVE/DEAD® Viability/Cytotoxicity Kit for mammalian cells (ref. L3224), Alamar Blue® (ref. DAL1025) and DAPI (ref. D21490) were supplied by Invitrogen. Human umbilical vein endothelial cells (HUVECs; cat. no. cc-2517) and endothelial growth medium (EGM; Clonetic, cat. no. cc-3124) were purchased from Lonza (Lonza Walker). Human foreskin fibroblasts HFF-1 (SCRC-1041) were purchased from the American Type Culture Collection (ATCC, USA). All cell culture plastic-ware and consumables were acquired from NUNC.

hMSCs and HFF1 were cultured in DMEM supplemented with 100 U mL^{-1} penicillin, 0.1 mg mL^{-1} streptomycin and 10 or 15 % FBS. HUVECs were grown in complete endothelial growth medium. Cells were incubated at 37 °C in a 5 % CO_2 humidified environmental chamber and their medium was replaced every 2 days.

2.8 Cell viability assays

2 × 105 HFF1 and 5 × 104 MSCs/mL were embedded inside ELR-CGs at a concentration of 50 mg/mL, as described previously. Metabolic activity was evaluated using the Alamar Blue® assay. The relative number of metabolically active cells was evaluated using the Alamar Blue® assay according to the manufacturer's guidelines. Twenty-four hours after seeding the cells, the hydrogels were washed twice with DPBS and incubated in 10 % Alamar Blue solution in DMEM for 2 h at 37 °C and under a 5 % CO_2 atmosphere. Subsequently, 70 μL of the reduced medium was transferred to a 96-well plate. The hydrogels were washed twice with DPBS, and the corresponding growth medium added and incubated again in order to determine the cell number at different times. Fluorescence (excitation: 560 nm; emission: 590 nm) was measured using a SpectraMax M5e (Molecular Devices) microplate reader. The fluorimetric reduction of 10 % Alamar Blue® reagent in the culture medium by the cells expressed as fluorescence emission intensity units, was measured at regular time intervals.

Samples for phase-contrast epifluorescence or SEM were fixed in 4 % paraformaldehyde for 40 min. The staining was carried out before permeabilization of the samples with 0.2 % Triton X-100, and stained with the fluorescent dyes Phalloidin-Alexa Fluor488R and DAPI, as indicated in the text.

2.9 Microstructural morphology

SEM in low vacuum mode (~1 torr) and with water vapour as working gas was used to investigate the morphology of both hydrogels and micropatterned hydrogels. ELR-CG hydrogels were immersed in milli-Q water below (at 4 °C) and above (at 37 °C) the Tt for 1 day, instantaneously plunged into liquid nitrogen, physically fractured, and immersed in liquid nitrogen again. Finally, the hydrogels were freeze-dried. Images of lyophilized hydrogels were obtained by SEM (FEI Quanta 200 FEG) without any coating procedures. Hydrogel microstructural details, such

as pore size and pore wall thickness, were quantitatively evaluated using the ZEN software (Blue Edition, 2012) from Carl Zeiss Microscopy based on the micrographs.

Structured hydrogels were peeled off from the mould after gelification and their surface topography observed without any treatment or manipulation.

2.10 Porosity and swelling ratio calculations

The following equation [36, 37] was employed to estimate hydrogel porosity:

$$\text{Porosity } (\%) = ((\text{W1} - \text{W2})/\rho \text{ water}) \cdot 100/\text{Vhydrogel} \quad (1)$$

where W1 and W2 are, respectively, the weight of swollen and lyophilized gel, ρwater is the density of pure water, and Vhydrogel is the measured volume of the gel in the swollen state (Vhydrogel = $\pi r^2 h$, where r and h are, respectively, the radius and height of the cylindrical sample). Excess surface water was removed with a filter paper before each measurement.

The equilibrium swelling ratio by weight, Qw, was used to quantify the volume change related to the phase transition of the hydrogels in aqueous solution.

$$\text{Qw } (\%) = ((\text{W1} - \text{W2})/\text{W2}) \cdot 100 \quad (2)$$

Both porosity and equilibrium swelling ratio were measured at 4° and 37 °C. All measurements were taken 24 h after soaking the hydrogel in MQ water at the chosen temperature. Equilibrium was defined as the steady state at which there was no change in volume of the ELR-CG. Lyophilization or freeze-drying was performed with hydrogels previously frozen in liquid nitrogen and swollen in water at the corresponding test temperature.

2.11 Rheological measurements

Rheological experiments were performed using a strain-controlled AR-2000ex rheometer (TA Instruments) with the hydrogel immersed in water. Cylindrical swollen gels were placed between parallel, nonporous stainless-steel plates (diameter = 12 mm) and the gap between the plates adjusted using a normal force of around 0.2 N in order to prevent slippage. A gap higher than 1,000 μm was always reached after the sample relaxed until equilibrium. Measurements were carried out at 4 °C and at 37 °C. Two types of measurements were performed in shear deformation mode. First of all, the range of strain amplitudes for which gels exhibit a linear region of viscoelasticity was determined. A dynamic strain sweep (with amplitudes ranging between 0.1 and 20 %) was carried out at a frequency of 1 Hz to measure the dynamic shear modulus as a function of strain. Second, in order to measure the dependence of the dynamic shear modulus and loss factor on frequency, dynamic frequency sweep tests were accomplished. Specifically, a frequency sweep between 0.01 and 10 Hz at a fixed strain (corresponding to the hydrogel linear region) was selected. Thus, the storage modulus, G′, the loss modulus, G′, the complex modulus magnitude, |G*| (|G*|2 = (G′)2 + (G″)2), and the loss factor, tan δ (tan δ ≡ G″/G′, where δ is the phase angle between the applied stimulus and the corresponding response) as a function of strain amplitude or frequency were obtained.

2.12 Statistical analysis

Data are reported as mean ± SD ($n = 3$). Error bars represent the standard deviation calculated from tests of triplicate measurements for each hydrogel at each recombinamer concentration. Statistical analysis was evaluated by a one-way analysis of variance using the Holm-Sidak method. A P value lower than 0.05 was considered to be statistically significant. ** $P < 0.001$, * $P < 0.05$, and $P > 0.05$ indicates no significant differences (n.s.d.).

3 Results and discussion

3.1 SEM measurements

SEM micrographs of ELR-CG hydrogels at 37 °C have been included in Fig. 2. A homogeneous 3D structure with high interconnectivity and a thin pore wall is observed for the lowest polymer concentration. Interconnectivity provides a noticeable advantage in tissue engineering applications, thereby favouring cell migration and nutrient delivery. The structure becomes denser and more compact, with a thicker pore wall, with increasing polymer concentration. As a consequence, porosity qualitatively decreases. A predominantly closed-pore structure is observed at higher concentrations, whereas an open-pore structure is found for low polymer concentrations. Both the mean pore size and mean pore wall thickness were evaluated and the results at 37 °C are included in Table 1. Pore geometry is predominantly circular or ellipsoidal, with pore size decreasing as ELR concentration increases. The pore wall thickness tends to increase as the recombinamer concentration increases. Both effects affect the porosity of the gels as defined in Eqs. 1 and 2 as will be demonstrated below.

3.2 Porosity and swelling ratios

The dependence of the ELR-CG hydrogel porosity on polymer concentration is plotted in Fig. 3a. In agreement with the SEM micrographs, hydrogel porosity decreases at both temperatures (37 and 4 °C) as concentration increases.

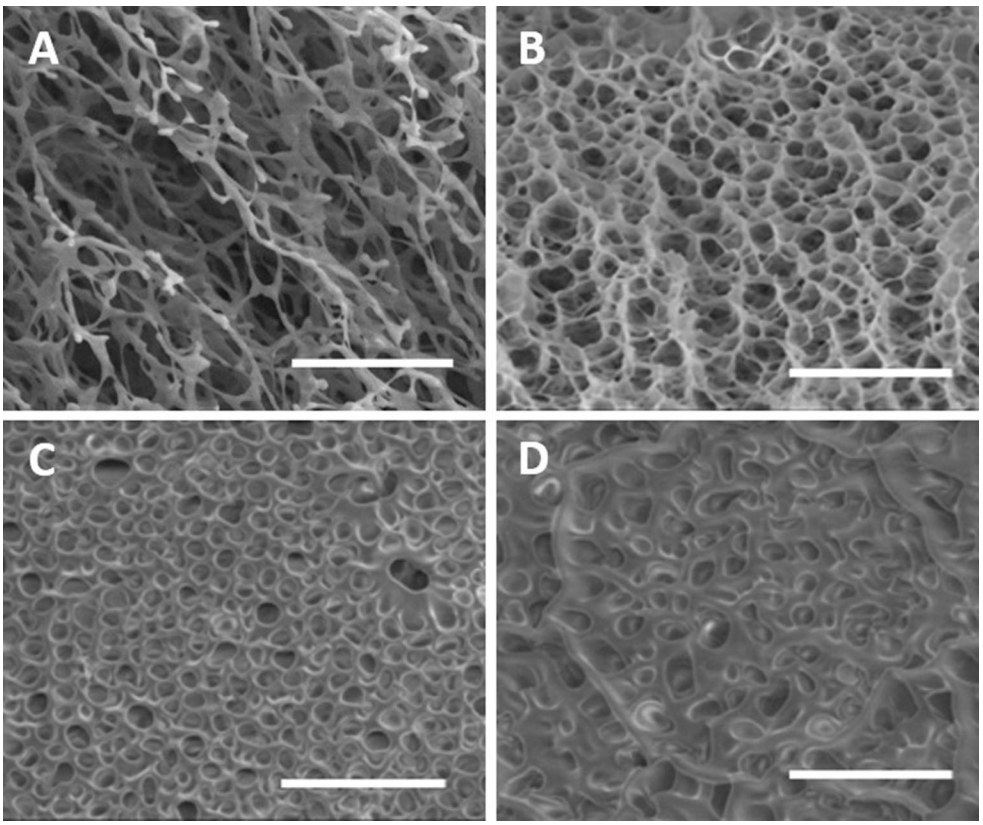

Fig. 2 Representative SEM micrographs for several polymer concentrations of ELR-CG hydrogels: 25 mg/mL (**a**), 50 mg/mL (**b**), 100 mg/mL (**c**), and 125 mg/mL (**d**) at 37 °C. *Scale bar* 20 μm

Table 1 Mean pore size and mean pore wall thickness at 37 °C for the ELR-CG hydrogels evaluated using the ZEN software (Blue Edition, 2012) from Carl Zeiss Microscopy. Thirty measurements taken in three different sample regions were averaged to calculate the mean and standard deviation values. $P < 0.05$ for pairwise multiple comparison between different concentrations

ELR-CG (mg/mL)	Pore size (μm)	Pore wall thickness (μm)
25	3.3 ± 0.7	0.4 ± 0.1
50	2.7 ± 0.3	0.5 ± 0.2
100	2.4 ± 0.3	1.1 ± 0.6
125	1.7 ± 0.4	2.1 ± 1.1

Porosity is higher at 4 °C than at 37 °C for a given concentration, although a high porosity is found at both temperatures. Specifically, a porosity value of around 70–75 % is found at 4 °C for a recombinamer concentration of 50 mg/mL. Furthermore, these results show that the hydrogel matrix retains the thermoresponsive nature of the original ELR. As can be seen from Fig. 3b, the equilibrium hydrogel swelling ratio at a given temperature decreases as the concentration increases. Although this trend is similar at both temperatures, in agreement with the literature [38] it is more evident at 4 °C. As the concentration increases, the number of polymer chains and the number of crosslinked chains also increases. Consequently, the ability of the hydrogel to swell is reduced.

Porosity and equilibrium swelling of the 125 mg/mL ELR-CG hydrogel at both temperatures are quite similar to the values found for the 100 mg/mL hydrogel. Covalent crosslinking requires both the presence of the reactive groups responsible for chain crosslinking and their accessibility. Moreover, a Cu(I) ion must be present to catalyse the ELR-CGs formation. At the highest concentration, where the number of polymer chains is very high, steric hindrance may limit the interaction between the groups that take part in the crosslinking process.

3.3 Rheological measurements

The viscoelastic mechanical properties of hydrogels have been determined by rheological measurements in the linear viscoelastic range using a strain of 1 %. The evolution of G', G'', and tan δ with frequency at 4 and 37° C has been also obtained, and both G' and G'' are frequency-dependent (data not shown). A similar frequency-dependence has been reported for biological tissue (e.g., liver [39] and uterus [40]) and newly synthesized materials [41, 42].

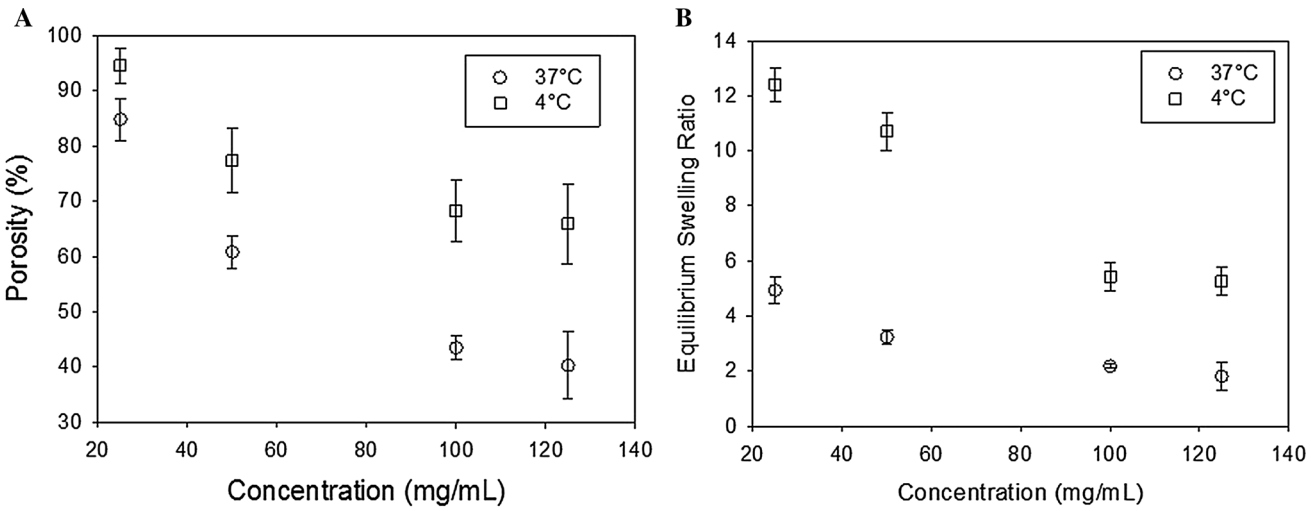

Fig. 3 Evolution of porosity (**a**) and equilibrium swelling ratio (**b**) as a function of polymer concentration for the ELR-CHG hydrogels at 4 and 37 °C. Data are reported as mean ± SD ($n = 3$)

The values of G′, G″, and tan δ as a function of polymer concentration are plotted in Fig. 4 at a fixed frequency of f = 1 Hz. As G′ is much larger than G″, the storage modulus is the dominant contribution to |G*|. The value of G′ at 1 Hz is in the range 1–10 kPa, tending towards the higher end of this range at the highest concentrations used. As such, the hydrogel exhibits a high degree of elasticity and the material can therefore be included in the category of "hard hydrogel". G′ and G″ increase with polymer concentration at both temperatures. However, the G′ value for the highest concentration shows some saturation (Fig. 4a). The same trend is observed at 4 and 37 °C. The porosity and swelling ratio results showed similar behaviour for this specific concentration.

Relatively similar values of G′ are found at both temperatures. Specifically, almost identical values are obtained at 4 and 37 °C for concentrations of 25 and 50 mg/mL. For higher concentrations, G′ is higher at 37 °C. These results can be explained by taking into account the high porosity observed for these samples [37]. Biomaterials with elastic moduli in the 1–10 kPa range are of widespread interest as many native tissues, for instance pig adventitial layer (4.7 ± 1.7 kPa) [43], canine kidney cortex and medulla (∼10 kPa), and nucleus pulpous and eye lens (∼1 kPa) [44], have moduli in this range. The moduli of isolated chondrocytes without cell-associated pericellular matrix have been reported to be in the range 0.6–4 kPa [45]. As far as the loss factor is concerned, no noticeable dependence on polymer concentration at a given temperature is observed from Fig. 4c. Tangent values of around 0.02 (at 4 °C) and 0.06 (at 37 °C) correspond to phase angles of about 1° and 3°, respectively. These values agree with the values for human bone (typically between 0.02 and 0.04) at physiological frequencies (around 10^{-2}–10^{3} Hz) [46]. Very low phase angles are characteristic of highly elastic, energy-storing hydrogels. At 4 °C these angles suggest low contact between the polymer chains. At 37 °C the hydrogels are contracted and shed water, thus meaning that far less water is present to lubricate chain reorientation in response to an applied strain. Values of tan δ at this temperature suggest that some portion of the load is transferred between interacting ELP chains by friction [38]. Our experimental results agree with the literature [47, 48] as, in general, tan δ does not correlate with either porosity or pore size.

3.4 Micropatterning of the ELR-CGs

It is well known that surface topography induces and controls cell behaviour [49, 50] and organization. As such, spatial control of the surface of materials for cell applications is a crucial factor to be taken into consideration when designing a device that will emulate the natural cell environment [51]. In light of this, several micropatterned gels, obtained by the replica moulding method, have been prepared for a recombinamer concentration of 50 mg/mL. Optical micrographs of the four different patterns obtained at 37 °C, as described previously, are shown in Fig. 5. The replication quality with respect to the original silicon masters is high, and the homogeneity over the whole area is remarkable. In light of these results, we can conclude that total control of the surface topography of these ELR-CHGs is possible using the simple replica moulding method.

3.5 Bioactivity

To evaluate the cytocompatibility of these new ELR-CGs, a polymer concentration of 50 mg/mL was chosen to form hydrogels with storage modulus values similar to those

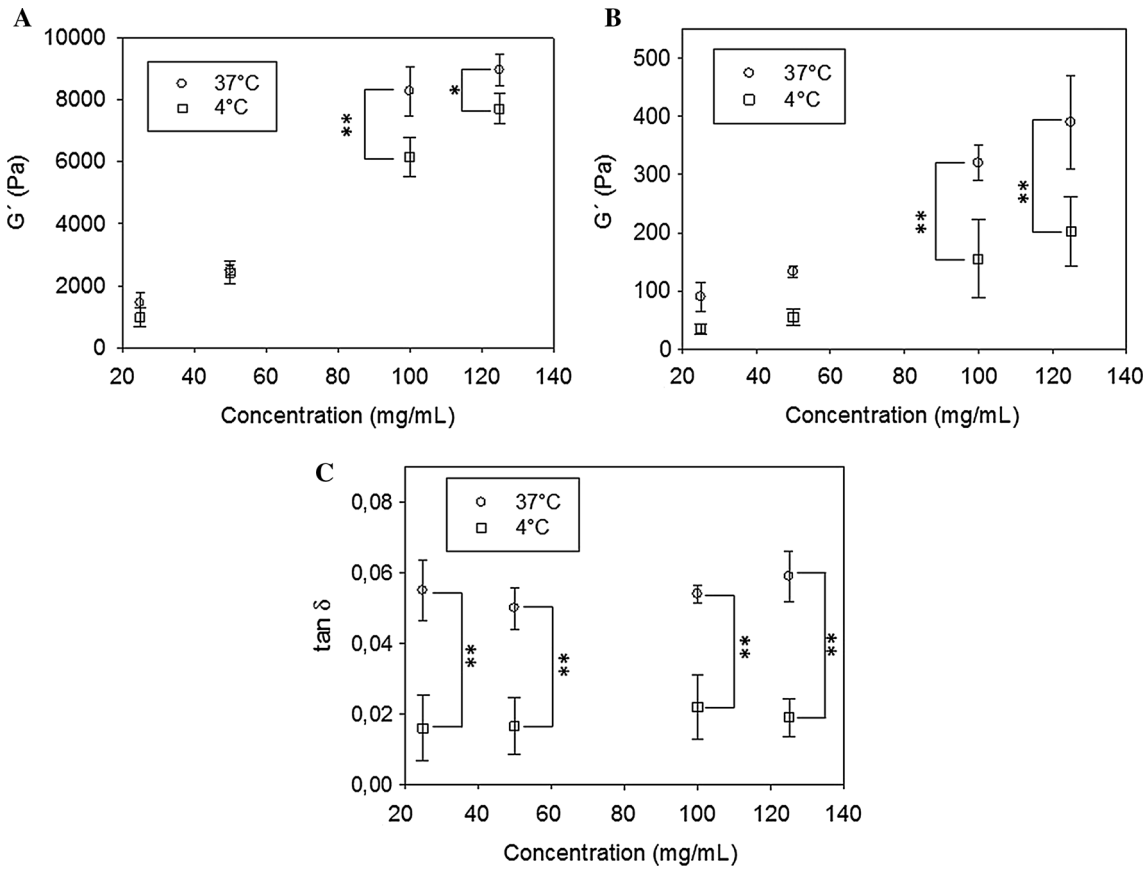

Fig. 4 Evolution of G′ (**a**), G″ (**b**), and tan δ (**c**) as a function of hydrogel polymer concentration at a fixed frequency of 1 Hz at 4° and 37 °C. Data are reported as mean ± SD ($n = 3$). Statistical analysis was performed using an analysis of variance with the Holm-Sidak method. $^{**}P < 0.001$, $^{*}P < 0.05$

found in many natural tissues, as mentioned above. Moreover, at this concentration the hydrogel combines high porosity, which is important for a good cell colonization of the material, with easy handling.

With the aim of determining the influence of the bioactive sequences in the backbone structure of the ELRs that form the ELR-CGs on cell adhesion and proliferation, two kinds of ELR-CGs were prepared: one lacking a bioactive sequence (VKV-CG) and the second including the well-known RGD cell-adhesion sequence (RGD-CG).

SEM pictures of the RGD-CGs surfaces after fibroblast seeding showed that the presence of RGD in the ELR backbone results in a strong adhesion of seeded cells that spread well on the hydrogel surfaces, as can be seen from Fig. 6. These findings corroborate those previously observed for films or nanofibre RGD-ELR scaffolds [22, 52, 53]. The first picture shows the gel surface prior to cell deposition, whereas pictures B and C show details of the surface after cell adhesion. Cells can be observed as a soft tissue covering the RGD-CG surface. ELR-CGs would allow the co-seeding of cellular and polymeric suspensions to form a hydrogel with embedded cells within a few minutes. In order to corroborate the viability of this process, gels were prepared and HFF-1 cells embedded inside the ELR-CGs as described previously. Metabolic activity tests were performed every 3 days for 18 days with the aim of evaluating the viability and proliferation of the embedded cells. As can be seen in Fig. 7, the viability of the HFF1 cells in RGD-CGs is clearly higher than in VKV-CGs for the whole culture time. The cells cultured in control CGs showed a lower metabolic activity that did not increase substantially during the experimental time. In contrast, fibroblasts embedded in RGD-CGs showed a sigmoidal growth, with slow growth in the first eight days, logarithmic growth between days nine and twelve, and stabilization until the end of the experiments. Although the presence of RGD in the molecule backbone of these scaffolds has no influence on the number of cells as they are encapsulated in the CGs, it is well known that binding between cell-surface receptors and ECM protein motifs activates the intracellular signalling pathways that strongly influence a cell's behaviour and fate [54]. In order to assess the ability of ELR-CGs to sustain different cell types, the development and phenotype of human primary cell cultures

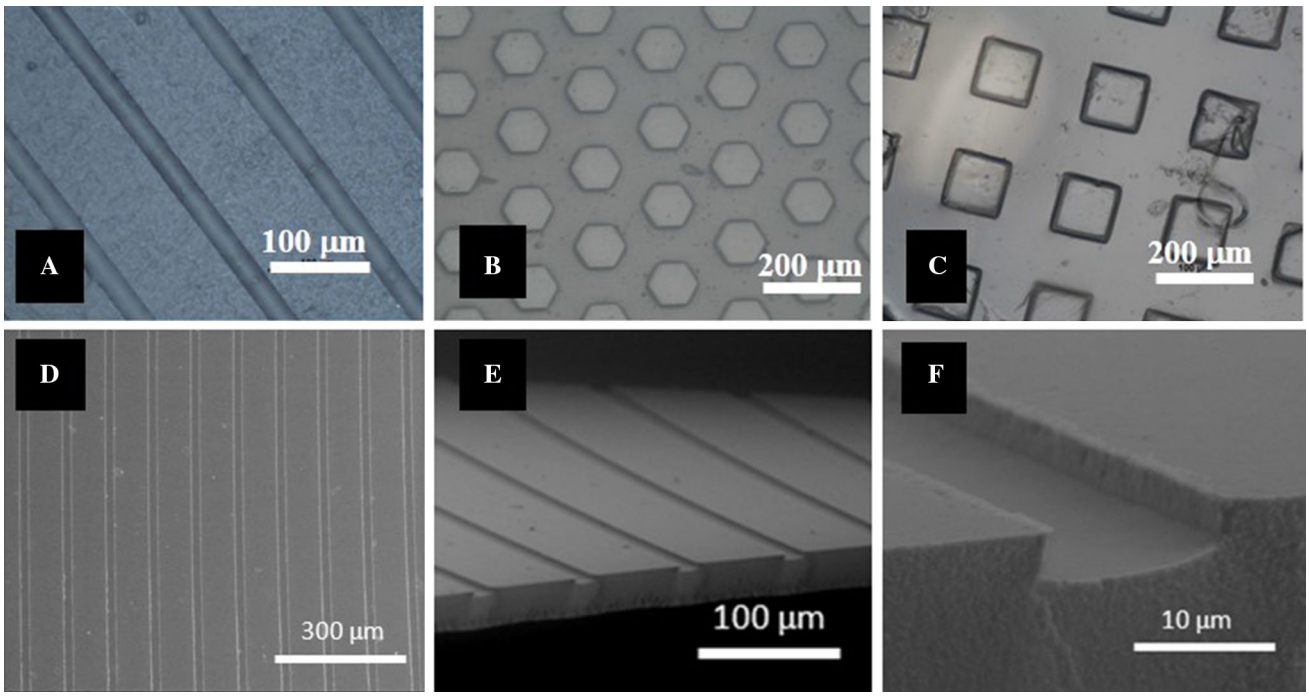

Fig. 5 Optical micrographs of micro-structured ELR-CGs at 37 °C (recombinamer concentration: 50 mg/mL) after demoulding. **a** 100 µm periodic grooves with w = 20 µm, **b** 100 µm periodic *hexagonal pillars* with w = 100 µm, **c** 100 µm periodic *square pillars* with w = 100 µm. **d**, **e**, and **f** SEM details of the micropatterned gel obtained in low vacuum mode for 100 µm periodic grooves with a width of 20 µm, and a step height (**h**) of 5 µm

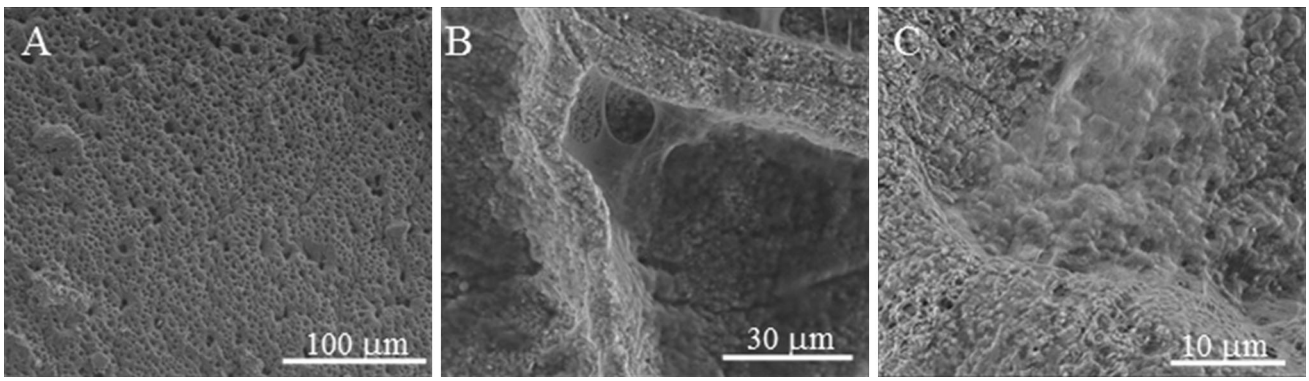

Fig. 6 SEM details of RGD-CGs prior to (**a**) and after (**b**, **c**) HFF-1 cell colonization

in click-hydrogels was evaluated. Primary cells were chosen as the model as they produce more physiologically relevant data than other cell lines. A one-week ELR-CGs culture of fibroblast, endothelial and mesenchymal stem cells was evaluated by optical fluorescent microscopy after hydrogel fixation and specific staining of the cytoskeletal actin (green) and nucleus (blue). As can be seen in Fig. 8, the embedded cells present in different focal planes have the typical morphology of their respective cell types, in other words large mesenchymal stem cells, extended, elongated and fibrous fibroblasts that can provide long cytoplasmic processes, and a polyhedral morphology for HUVECs. MSCs are pluripotent cells that are able to differentiate into multiple cells types widely utilized in both tissue engineering and regenerative medicine. Long-term culture studies were carried out with MSCs embedded inside RGD-CGs obtained as described previously, with cells seeded on standard polystyrene cell culture being used as controls. The metabolic activity of these cells was measured for 60 days. As can be seen from Fig. 9, cell growth shows a sigmoidal behaviour, with slow growth for the first 10–15 days. This first phase is followed by a logarithmic growth phase from day 20 onwards. The delayed growth in the ELR-CG observed in the first phase is compensated in

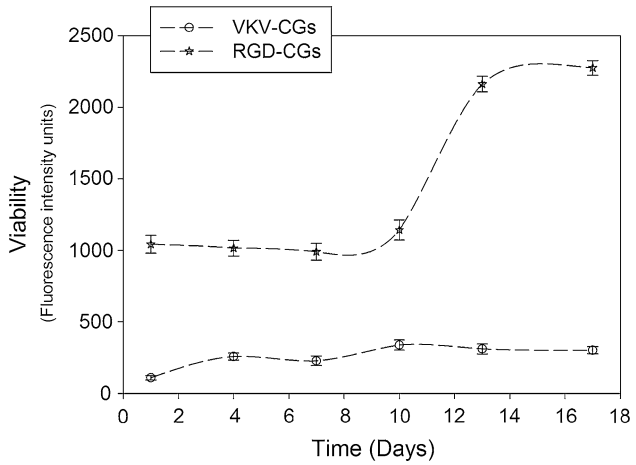

Fig. 7 Dependence of viability of HFF-1 cells on two different substrates containing or lacking the bioactive sequence RGD (VKV-CGs and RGD-CGs) over 18 days. *Error bars* represent standard error ($n = 4$)

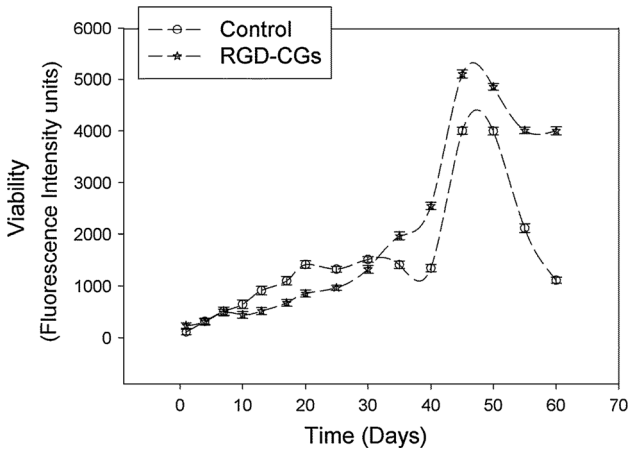

Fig. 9 Dependence of MSC viability in RGD-CGs over 60 days. Comparison of growth on standard plastic tissue culture and cells embedded inside ELR-CGs. Error bars represent standard error ($n = 4$)

this second phase and is followed by a higher metabolic stability of the cells in the last stationary phase in the ELR-CG than for the control. Figure 10 shows a morphological analysis of the MSCs embedded in the three-dimensional structure. Although the texture, consistency and thickness of the gel partially hinder viewing, embedded cells can be analysed in different focal planes in which we can see extended and elongated cells with long cytoplasmic processes. Colonization of the hydrogel is almost complete after 60 days, thus indicating that the scaffolds are capable

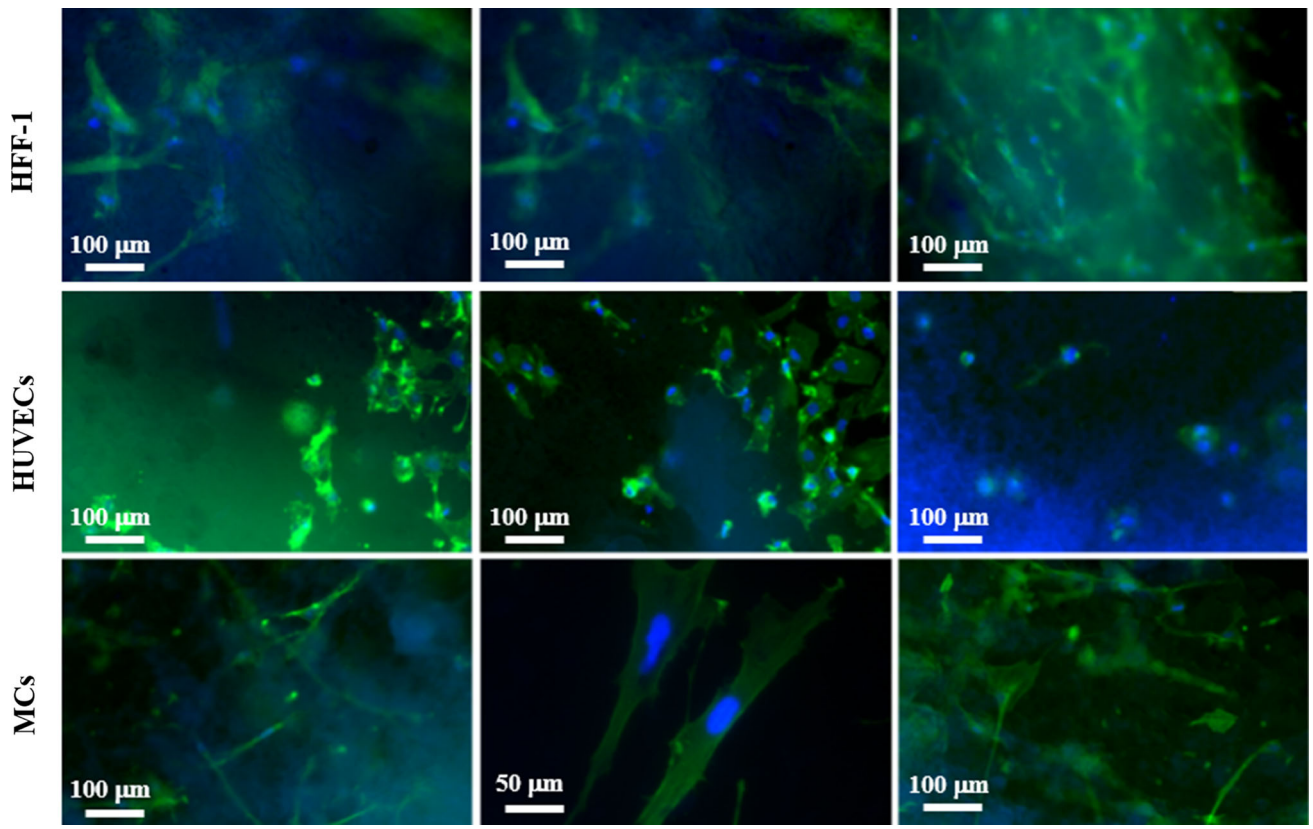

Fig. 8 Human primary fibroblasts (HFF1), human primary umbilical vein endothelial cells (HUVEC) and human adipose-derided tissue mesenchymal stem cells (MSC) embedded inside RGD-CGs after 7 days of culture

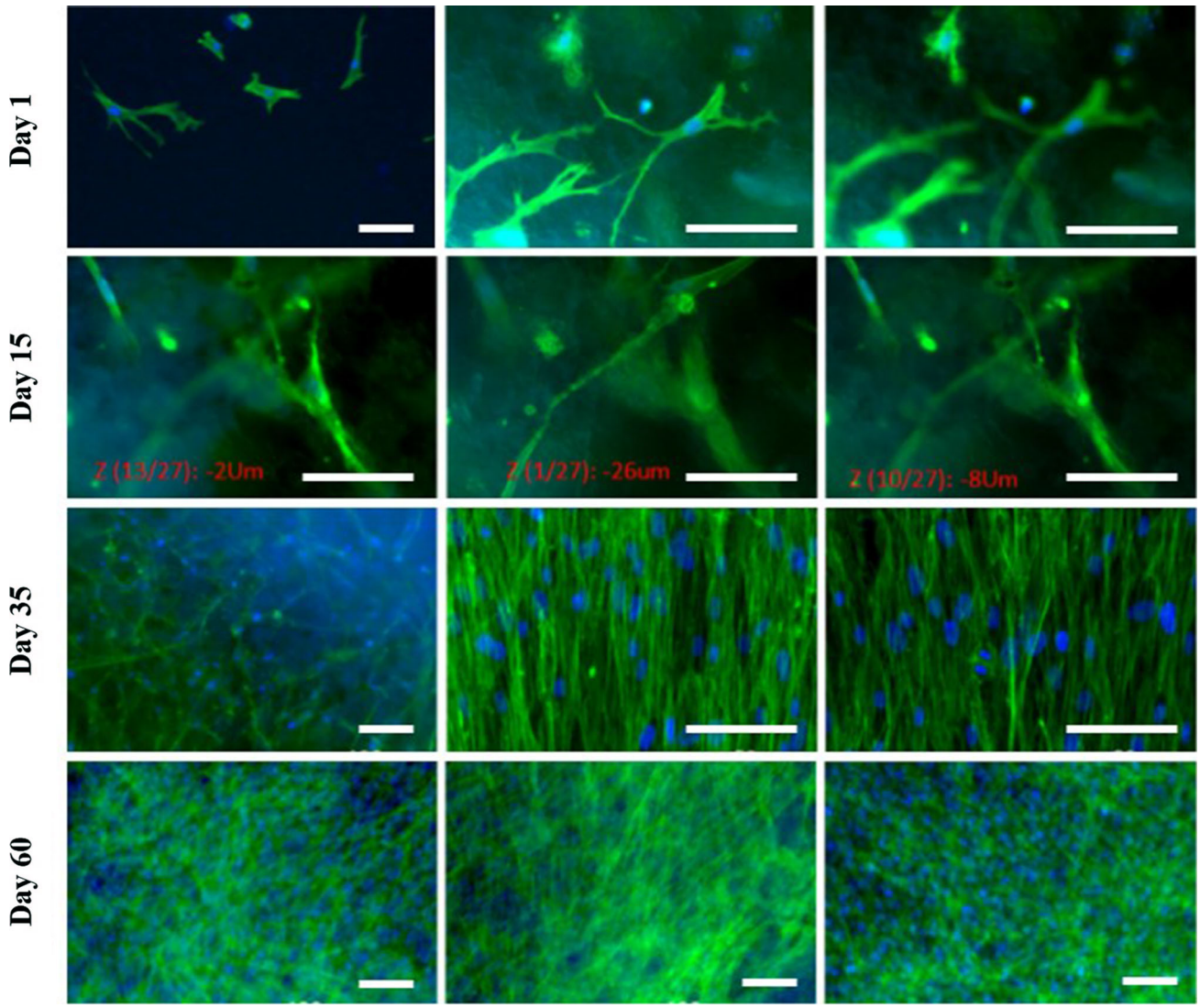

Fig. 10 Optical microscope pictures of RGD-CG colonization by MSCs in several focal *planes* for up to 60 days. *Scale bars* 100 μm

of supporting the long-term culture of embedded cells. The protein nature of the ELR-CGs could allow the cell-mediated remodeling of the artificial scaffold due to the proteases action during the new extracellular matrix synthesis, permitting the cell proliferation, and thus, a quite total colonization of the scaffolds. Cells showed a well-spread morphology, with large extensions and numerous pseudopodia, and their cytoskeleton actin filaments (green stained) were well organized in stress fibres, thereby indicating a strong adhesion.

In this paper two ELRs, namely a structural ELR (VKVx24) and an ELR containing the RGD cell-adhesion sequence (HRGD6) have been chemically modified at the amino groups of the lysine residues to bear azide and alkyne groups that react in the presence of Cu(I) to yield novel and highly biocompatible elastin-like recombinamer-click hydrogels (ELR-CGs). These ELR-CGs have been designed, synthesized, and characterized, and their cytocompatibility has also been tested. Special attention has been paid to their microstructural morphology and mechanical properties, and the correlation between SEM micrographs, porosity, swelling ratio, rheological measurements and concentration has been determined. We have reported a simple, fast, water-based method for obtaining micropatterned ELR-CGs under mild, physiological conditions by replica moulding. This ELR-CGs system enables the highly reproducible fabrication of different microstructured surfaces and can be used as a substrate with a well-controlled microtopography for studying spatially controlled cell behaviour. Injectable hydrogels present several important therapeutic advantages as regards the minimally invasive implantation technique, reducing the pain associated with

conventional surgical procedures. The possibility of co-injection of cells as therapeutic agents that remain embedded and confined at the administration site is another great benefit of this approach.

Studies of the medium- and long-term viability have revealed a good cytocompatibility with respect to several human primary cell types (HFF-1, MSCs and HUVECs) in both surface and 3D cultures. As such, we can conclude that our ELR-CGs are able to maintain and expand cell cultures in time and are therefore suitable scaffolds for tissue engineering.

Several polymer concentrations and temperatures have been used to obtain gels with fully tuneable properties with potential applications as drug-delivery systems or scaffolds for tissue engineering.

Acknowledgments We acknowledge financial support from the EU via the European regional development fund (ERDF), from the MINECO (MAT-2010-15982, MAT2010-15310, PRI-PIBAR-2011-1403 and MAT2012-38043), the JCyL (Projects VA049A11, VA152A12 and VA155A12), the CIBER-BBN, and the JCyL and the Instituto de Salud Carlos III under the "Network Center of Regenerative Medicine and Cellular Therapy of Castilla and Leon".

References

1. Mitragotri S, Lahann J. Physical approaches to biomaterial design. Nat Mater. 2009;8(1):15–23.
2. Raghavan S, Chen CS. Micropatterned environments in cell biology. Adv Mater. 2004;16(15):1303–13.
3. Curtis A, Wilkinson C. Topographical control of cells. Biomaterials. 1997;18(24):1573–83.
4. Falconnet D, Csucs G, Grandin HM, Textor M. Surface engineering approaches to micropattern surfaces for cell-based assays. Biomaterials. 2006;27(16):3044–63.
5. Curtis A, Wilkinson C. Topographical control of cells. Biomaterials. 1997;18(24):1573–83.
6. Mata A, Boehm C, Fleischman AJ, Muschler G, Roy S. Analysis of connective tissue progenitor cell behavior on polydimethylsiloxane smooth and channel micro-textures. Biomed Microdevices. 2002;4(4):267–75.
7. Mata A, Kim EJ, Boehm CA, Fleischman AJ, Muschler GF, Roy S. A three-dimensional scaffold with precise micro-architecture and surface micro-textures. Biomaterials. 2009;30(27):4610–7.
8. Dalby MJ, Gadegaard N, Tare R, Andar A, Riehle MO, Herzyk P, Wilkinson CD, Oreffo RO. The control of human mesenchymal cell differentiation using nanoscale symmetry and disorder. Nat Mater. 2007;6(12):997–1003.
9. Engler AJ, Sen S, Sweeney HL, Discher DE. Matrix elasticity directs stem cell lineage specification. Cell. 2006;126(4):677–89.
10. Rodríguez-Cabello JC, Martín L, Alonso M, Arias FJ, Testera AM. "Recombinamers" as advanced materials for the post-oil age. Polymer. 2009;50(22):5159–69.
11. Arias FJ, Santos M, Fernandez-Colino A, Pinedo G, Girotti A. Recent contributions of elastin-like recombinamers to biomedicine and nanotechnology. Curr Topic Med Chem. 2014;14(6):819–36.
12. Rincón A, Molina-Martinez I, de Las Heras B, Alonso M, Baílez C, Rodríguez-Cabello J, Herrero-Vanrell R. Biocompatibility of elastin-like polymer poly(VPAVG) microparticles: in vitro and in vivo studies. J Biomed Mater Res. 2006;78(2):343–51.
13. Wright ER, Conticello VP. Self-assembly of block copolymers derived from elastin-mimetic polypeptide sequences. Adv Drug Deliv Rev. 2002;54(8):1057–73.
14. Kolb HC, Finn MG, Sharpless KB. Click chemistry: diverse chemical function from a few good reactions. Angew Chem Int Edition. 2001;40(11):2004–21.
15. Meldal M, Tornøe CW. Cu-catalyzed azide − alkyne cycloaddition. Chem Rev. 2008;108(8):2952–3015.
16. Tornøe CW, Christensen C, Meldal M. Peptidotriazoles on solid phase: [1,2,3]-triazoles by regiospecific copper(I)-catalyzed 1,3-dipolar cycloadditions of terminal alkynes to azides. J Org Chem. 2002;67(9):3057–64.
17. Rostovtsev VV, Green LG, Fokin VV, Sharpless KB. A stepwise huisgen cycloaddition process: copper(I)-catalyzed regioselective "Ligation" of azides and terminal alkynes. Angew Chem Int Edition. 2002;41(14):2596–9.
18. Devlieger R, D'Hooghe T, Timmerman D. Uterine adenomyosis in the infertility clinic. Hum Reprod Update. 2003;9(2):139–47.
19. Baskin JM, Prescher JA, Laughlin ST, Agard NJ, Chang PV, Miller IA, Lo A, Codelli JA, Bertozzi CR. Copper-free click chemistry for dynamic in vivo imaging. Proc Natl Acad Sci. 2007;104(43):16793–7.
20. Wenge U, Ehrenschwender T, Wagenknecht H-A. Synthesis of 2′-*O*-propargyl nucleoside triphosphates for enzymatic oligonucleotide preparation and "click" modification of dna with nile red as fluorescent probe. Bioconjugate Chem. 2013;24(3):301–4.
21. Laughlin ST, Baskin JM, Amacher SL, Bertozzi CR. In vivo imaging of membrane-associated glycans in developing zebrafish. Science. 2008;320(5876):664–7.
22. Pierna M, Santos M, Arias FJ, Alonso M, Rodríguez-Cabello JC. Efficient cell and cell-sheet harvesting based on smart surfaces coated with a multifunctional and self-organizing elastin-like recombinamer. Biomacromolecules. 2013;14(6):1893–903.
23. Ossipov DA, Hilborn J. Poly(vinyl alcohol)-based hydrogels formed by "Click Chemistry". Macromolecules. 2006;39(5):1709–18.
24. Jiang Y, Chen J, Deng C, Suuronen EJ, Zhong Z. Click hydrogels, microgels and nanogels: emerging platforms for drug delivery and tissue engineering. Biomaterials. 2014;35(18):4969–85.
25. Urry DW, Pattanaik A, Xu J, Woods TC, McPherson DT, Parker TM. Elastic protein-based polymers in soft tissue augmentation and generation. J Biomater Sci Polym Ed. 1998;9(10):1015–48.
26. Urry DW, Parker TM, Reid MC, Gowda DC. Biocompatibility of the bioelastic materials, poly(gvgvp) and its γ-irradiation cross-linked matrix: summary of generic biological test results. J Bioact Compat Polym. 1991;6(3):263–82.
27. Lampe KJ, Antaris AL, Heilshorn SC. Design of three-dimensional engineered protein hydrogels for tailored control of neurite growth. Acta Biomate. 2013;9(3):5590–9.
28. Betre H, Setton LA, Meyer DE, Chilkoti A. Characterization of a genetically engineered elastin-like polypeptide for cartilaginous tissue repair. Biomacromolecules. 2002;3(5):910–6.
29. Betre H, Ong SR, Guilak F, Chilkoti A, Fermor B, Setton LA. Chondrocytic differentiation of human adipose-derived adult stem cells in elastin-like polypeptide. Biomaterials. 2006;27(1):91–9.
30. Tejeda-Montes E, Smith KH, Poch M, López-Bosque MJ, Martín L, Alonso M, Engel E, Mata A. Engineering membrane scaffolds with both physical and biomolecular signaling. Acta Biomater. 2012;8(3):998–1009.
31. Martin L, Alonso M, Moller M, Rodriguez-Cabello JC, Mela P. 3D microstructuring of smart bioactive hydrogels based on recombinant elastin-like polymers. Soft Matter. 2009;5(8):1591–3.
32. Martin L, Arias FJ, Alonso M, Garcia-Arevalo C, Rodriguez-Cabello JC. Rapid micropatterning by temperature-triggered reversible gelation of a recombinant smart elastin-like tetrablock-copolymer. Soft Matter. 2010;6(6):1121–4.

33. Rodriguez-Cabello JC, Girotti A, Ribeiro A, Arias FJ. Synthesis of genetically engineered protein polymers (recombinamers) as an example of advanced self-assembled smart materials. Methods Mol Biol. 2012;811:17–38 (Clifton, N.J.).
34. Costa RR, Custodio CA, Arias FJ, Rodriguez-Cabello JC, Mano JF. Layer-by-layer assembly of chitosan and recombinant biopolymers into biomimetic coatings with multiple stimuli-responsive properties. Small. 2011;7(18):2640–9.
35. Lundquist IV, Pelletier JC. Improved solid-phase peptide synthesis method utilizing α-azide-protected amino acids. Org Lett. 2001;3(5):781–3.
36. Zeng X, Ruckenstein E. Control of pore sizes in macroporous chitosan and chitin membranes. Ind Eng Chem Res. 1996;35(11): 4169–75.
37. Martin L, Alonso M, Girotti A, Arias FJ, Rodriguez-Cabello JC. Synthesis and characterization of macroporous thermosensitive hydrogels from recombinant elastin-like polymers. Biomacromolecules. 2009;10(11):3015–22.
38. Trabbic-Carlson K, Setton LA, Chilkoti A. Swelling and mechanical behaviors of chemically cross-linked hydrogels of elastin-like polypeptides. Biomacromolecules. 2003;4(3):572–80.
39. Kiss MZ, Varghese T, Hall TJ. Viscoelastic characterization of in vitro canine tissue. Phys Med Biol. 2004;49(18):4207–18.
40. Kiss MZ, Hobson MA, Varghese T, Harter J, Kliewer MA, Hartenbach EM, Zagzebski JA. Frequency-dependent complex modulus of the uterus: preliminary results. Phys Med Biol. 2006;51(15):3683–95.
41. Oliveira MB, Song W, Martin L, Oliveira SM, Caridade SG, Alonso M, Rodriguez-Cabello JC, Mano JF. Development of an injectable system based on elastin-like recombinamer particles for tissue engineering applications. Soft Matter. 2011;7(14): 6426–34.
42. de Torre IG, Santos M, Quintanilla L, Testera A, Alonso M, Rodríguez-Cabello JC. Elastin-like recombinamer catalyst-free click gels: characterization of poroelastic and intrinsic viscoelastic properties. Acta Biomater. 2014;10(6):2495–505.
43. Yu Q, Zhou J, Fung YC. Neutral axis location in bending and Young's modulus of different layers of arterial wall. Am J Physiol. 1993;265(1):H52–60.
44. Erkamp RQ, Wiggins P, Skovoroda AR, Emelianov SY, O'Donnell M. Measuring the elastic modulus of small tissue samples. Ultrason Imaging. 1998;20(1):17–28.
45. Freeman PM, Natarajan RN, Kimura JH, Andriacchi TP. Chondrocyte cells respond mechanically to compressive loads. J Orthop Res. 1994;12(3):311–20.
46. Buechner PM, Lakes RS, Swan C, Brand RA. A broadband viscoelastic spectroscopic study of bovine bone: implications for fluid flow. Ann Biomed Eng. 2001;29(8):719–28.
47. Spiller KL, Laurencin SJ, Charlton D, Maher SA, Lowman AM. Superporous hydrogels for cartilage repair: evaluation of the morphological and mechanical properties. Acta Biomater. 2008;4(1):17–25.
48. Ghosh S, Gutierrez V, Fernández C, Rodriguez-Perez MA, Viana JC, Reis RL, Mano JF. Dynamic mechanical behavior of starch-based scaffolds in dry and physiologically simulated conditions: effect of porosity and pore size. Acta Biomater. 2008;4(4):950–9.
49. Curtis A, Wilkinson C. Topographical control of cells. Biomaterials. 1997;18:1573–83.
50. Falconnet D, Csucs G, Grandin H, Textor M. Surface engineering approaches to micropattern surfaces for cell-based assays. Biomaterials. 2006;27(16):3044–63.
51. Martin L, Arias JF, Alonso M, Garcia-Arevalo C, Rodriguez-Cabello JC. Rapid micropatterning by temperature-triggered reversible gelation of a recombinant smart elastin-like tetrablock-copolymer. Soft Matter. 2010;6(6):1121–4.
52. Garcia-Arevalo C, Pierna M, Girotti A, Arias FJ, Rodriguez-Cabello JC. A comparative study of cell behavior on different energetic and bioactive polymeric surfaces made from elastin-like recombinamers. Soft Matter. 2012;8(11):3239–49.
53. Ozturk N, Girotti A, Kose GT, Rodríguez-Cabello JC, Hasirci V. Dynamic cell culturing and its application to micropatterned, elastin-like protein-modified poly(N-isopropylacrylamide) scaffolds. Biomaterials. 2009;30(29):5417–26.
54. Yannas IV. Emerging rules for inducing organ regeneration. Biomaterials. 2013;34(2):321–30.